PAPER

Check for updates

The effective removal of Pb²⁺ by activated carbon fibers modified by L-cysteine: exploration of kinetics, thermodynamics and mechanism

Lingkai Zhu,[ab] Yuyuan Yao,[b] Dingzhou Chen[c] and Ping Lan [iD] *[a]

Herein, we developed a low-cost fabrication route to prepare chemically grafted activated carbon fibers, which effectively removed Pb²⁺ from solution. Multiple characteristic results indicated that L-cyst-ACF had abundant nitrogen-containing and sulfur-containing functional groups. Based on the XPS and EDS analyses, the capture of Pb²⁺ was attributed to the abundant adsorption sites on the fiber surface. According to the analysis of the pseudo-second-order kinetic model and the Langmuir isotherm model, the adsorption process could be interpreted as monolayer adsorption and chemisorption, and the equilibrium adsorption capacity was determined to be 136.80 mg g⁻¹ by fitting the pseudo-second-order kinetic model. The maximum adsorption capacity of L-cyst-ACF for Pb²⁺ was calculated to be 179.53 mg g⁻¹ using the Langmuir model. In addition, the adsorption reaction was endothermic and spontaneous, as evidenced by the thermodynamic parameters. The outcomes of this study provide a low-cost and feasible strategy for the remediation of Pb²⁺ pollution in the environment.

1 Introduction

The rapid development of modern industry has produced a large amount of wastewater polluted with heavy metals, which has caused great ecological and environmental harm, and finally poses a threat to human health through the food chain.[1,2] Heavy metal ions are non-biodegradable carcinogenic factors and tend to accumulate in organisms.[3,4] Heavy metals can enter the food chain through plants and pose a serious threat to human health.[5] Common heavy metal ions can cause acute and chronic diseases such as digestive inflammation, brain injury and cancers.[6] Therefore, the removal of heavy metal ions from industrial wastewater has become a major pro-environmental problem in recent years.

Various technologies to remove heavy metals from water are available, such as solvent extraction,[7] ion exchange,[8] precipitation[9,10] and adsorption.[11] Among them, adsorption has the advantages of simple operation, high efficiency, and strong flexibility. Many materials have been used to remove heavy metals such as activated carbon,[12,13] polymers,[14,15] and nanomaterials.[16] However, the practical application of adsorbents is hindered by their low adsorption efficiency for the target metal, the inconvenient process for their synthesis of and their unachievable recycling. Therefore, the development of advanced adsorbents with high adsorption capacity, recyclability and good chemical stability has become a vital research direction in the field of heavy metal remediation.

Activated carbon fibers (ACFs) are a new type of adsorbent developed in recent years to remove pollutants in aqueous solutions. Compared with the traditional activated carbon particles, activated carbon fibers have more suitable pore sizes, better adsorption effect and easy recycling.[17–19] Javier[20] *et al.* measured the effect of activated carbon fibers to adsorb both Pb²⁺-phenol and Cd²⁺-phenol simultaneously, proving that the selectivity of activated carbon fibers for Pb²⁺ ions was greater than Cd²⁺ ions. Deng[18] *et al.* found that a novel thiosemicarbazide-modified adsorbent exhibited a high performance towards Cd(II) and Pb (II). This result explained that sulfur-containing groups and nitrogen-containing groups could effectively adsorb metal ions in solution by chelation and coordination.

In the present study, activated carbon fiber adsorbents grafted with multiple functional groups with high adsorption properties were prepared *via* a simple amide reaction. The preparation fibers were characterization through multiple technologies such as Fourier transform infrared spectroscopy (FT-IR), X-ray photoelectron spectroscopy (XPS), scanning electron microscopy (SEM) and energy dispersive X-ray analysis (EDX). Meanwhile, the behavior and mechanism of Pb²⁺ adsorption were comprehensively explored *via* adsorption kinetics, isotherm models, and thermodynamic parameters. Then, the adsorption performance of L-cyst-ACF for Pb²⁺ was systematically discussed, which suggested that the adsorption process was spontaneous and endothermic.

[a]College of Materials and Textile Engineering, Jiaxing University, Jiaxing, 314001, China. E-mail: LanPing007@126.com

[b]School of Materials Science and Engineering, Zhejiang Sci-Tech University, Hangzhou, 310018, China

[c]Zhejiang Yana Textile Co., Ltd, Haining 314400, China

2 Materials and methods

2.1 Materials

Activated carbon fibers were obtained from Jiangsu Sutong Carbon Fiber Co., Ltd (Suzhou, China). Thiourea (AR, 99%), *N*-(3-dimethylaminopropyl)-*N*′-ethyl-carbodiimide hydrochloride (EDC, AR, 99%), *N*-hydroxy-succinimide (NHS, AR, 99%), and NaHSO$_4$ (AR, 99%) were purchased from Aladdin Regent Co. Ltd (Shanghai, China). Pb (NO$_3$)$_2$ (AR, 99%) was produced from Sinopharm Chemical Reagent Co, Ltd (Shanghai, China). Na$_2$S (AR, 98%) was procured from Macklin Biochemical Technology Co., Ltd (Shanghai, China). Ethyl alcohol (AR, 99.9%) was bought from Jiangsu Qiangsheng Functional Chemistry Co., Ltd (Suzhou, China). Dichloromethane (AR, 99.5%) was produced from Hangzhou Shuanglin Chemical Reagent Co., Ltd (Hangzhou, China). HNO$_3$ (AR 65%) and H$_2$SO$_4$ (AR 98%) were bought from Sinopharm Chemical Reagent Co, Ltd (Shanghai, China). L-Cysteine hydrochloride monohydrate (AR 99%), KH$_2$PO$_4$ (AR 99.5%), and Na$_2$HPO$_4$ (AR 99%) were all bought from Aladdin Regent Co. Ltd (Shanghai, China).

2.2 Preparation of L-Cysteine-modified activated carbon fiber

Activated carbon fibers were washed with deionized water several times and dried for 12 h at 80 °C until a constant weight. Then, the clean fibers were cut into small pieces and soaked in a HNO$_3$/H$_2$SO$_4$ (3 : 1, *v* : *v*) solution for acidification. The fibers were washed several times and dried overnight. ACFs were put in an appropriate amount of KH$_2$PO$_4$/Na$_2$HPO$_4$ buffer solution with a pH of 8.5. EDC (1.8 g) and NHS (1.2 g) were added to the solution with constant stirring at room temperature, and then thiourea (1.52 g) was added. After 6 h, ACFs were washed and dried.

Firstly, 1.38 g of sodium bisulfate (NaHSO$_4$) was added to 100 mL of 0.1 m L^{-1} dilute hydrochloric acid solution, and then 80 mL of ethanol was added. Subsequently, ACF and L-cysteine (1.7563 g) were added to the above mixture, and the system was heated at reflux at 95 °C for 6 h. The product was washed with ethanol and deionized water several times, and then dried at 80 °C *in vacuo* for 24 h. To reduce the oxidized sulfhydryl group (–SH), ACFs were added to an organic solvent (dichloromethane:ethyl alcohol, *v* : *v* = 1 : 2), Na$_2$S was added to the mixture as a reducing agent, and then it was stirred at room temperature for a certain of time. Finally, ACFs were filtered and washed several times, and then stored after drying. The specific experimental steps are shown in Fig. 1.

2.3 Characterization of L-cyst-ACF

The properties of L-cyst-ACF were characterized *via* a series of performance tests. Fourier-transform infrared spectra (FTIR) were recorded in pressed KBr using a Vertex 70 spectrophotometer (Bruker) in the range of 500–4000 cm^{-1} at room temperature. The morphological characteristics of L-cyst-ACF were observed *via* SEM (Hitachi, SU8010). The elemental components of L-cyst-ACF before and after adsorption were identified by X-ray photoelectron spectroscopy (XPS, Thermo Fisher: ESCALAB 250Xi, single Al *K*α as the light excitation source). An Oxford X-MaxN scanning electron microscope (SEM)/energy dispersive X-ray spectroscopy (EDS) was used to observe the surface morphology and element distribution of the fiber, respectively. Inductively coupled plasma atomic emission spectrometry (ICP-MS Agilent: 7800, China) was used to detect the Pb(II) concentration.

2.4 Batch adsorption experiments

A sequence of batch adsorption experiments was conducted to investigate the performance of the synthesized adsorbents for the elimination of Pb^{2+} from aqueous solution. The adsorption experiments were performed in an SHA-B water bath oscillator (RongHua Instrument Manufacturing Co., Ltd, China) at a shaking speed of 120 rpm. Batch experiments were performed to investigate the kinetics, isothermal models, and thermodynamic parameters during the adsorption process. In this investigation, the initial metal ion concentration range was 0–500 mg L^{-1}, adsorbent dose range was from 50 to 150 mg and the system temperatures were 303 K, 313 K and 323 K, respectively. The pH range of 2–6 was adopted in the experiment to investigate the influence of pH. All batch experimental solution
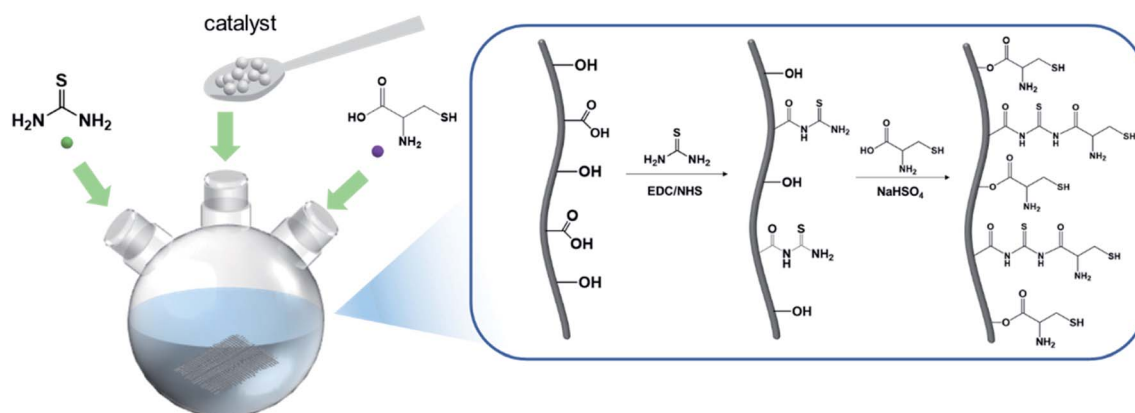

Fig. 1 Process for the preparation of cysteine-modified activated carbon fibers.

concentrations were detected through inductively coupled plasma atomic emission spectrometry. Before the solution concentration test, the test liquids were filtered with a 0.22 μm filter to remove impurities.

The adsorption amount q_e (mg g^{-1}) of Pb^{2+} in adsorption equilibrium was calculated using eqn (1):

$$q_e = \frac{(C_0 - C_e) \times V}{M} \tag{1}$$

The removal efficiency of Pb^{2+} at equilibrium was calculated using eqn (2):

$$\text{Removal (\%)} = \frac{C_0 - C_e}{C_0} \times 100\% \tag{2}$$

where C_0 and C_e are the initial concentration and equilibrium concentration (mg L^{-1}), respectively. V (L) is the volume of the solution and M (g) is the weight of the absorbent.

3   Results and discussion

3.1   Characterization of ACF and L-cyst-ACF

The FT-IR spectra of ACF and L-cyst-ACF are shown in Fig. 2. In the spectrum of the activated carbon fibers, the band at 3442 cm^{-1} is ascribed to the –OH stretching vibration[21] and that at 1654 cm^{-1} is ascribed to the C=O stretching.[22] The peaks at 1541 cm^{-1} and 1388 cm^{-1} correspond to the C–C and C–O bonds, respectively.[23] Similarly, the peak at 3446 cm^{-1} in the spectrum of L-cyst-ACF represents the –OH stretching vibration, and the two peaks at 1527 cm^{-1} and 1386 cm^{-1} can be ascribed to the C–C and C–O groups, respectively.[24] The peaks at 2813 cm^{-1} and 2933 cm^{-1} are attributed to the stretching vibrations of –CH$_2$ and –CH$_3$, respectively. The sharp peak at 3471 cm^{-1} and the broad band at around 3100–3300 cm^{-1} are attributed to the –NH$_2$ vibration.[25] Obviously, the sharp peak at
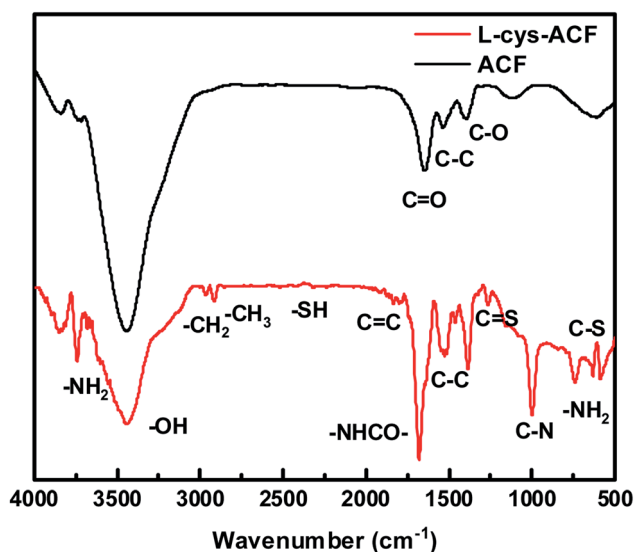
1655 cm^{-1} can be assigned to the carbonyl stretch of the –NHCO– group, not just the carbonyl group (C=O).[24] Meanwhile, a weak peak located at 2401 cm^{-1} was observed, which can be attributed to the –SH bending vibration.[18,26] The small peak at 1267 cm^{-1} is ascribed to the C=S bond.[12] The band at 1000 cm^{-1} may be caused by the C–N stretching.[27] In addition, the peaks at 740 cm^{-1} and 632 cm^{-1} correspond to the bending vibration of –NH$_2$ and vibrational C–S bonds, respectively.[28]

3.2   Characterization of ACF-SH

The SEM images of ACF and L-cyst-ACF are shown in Fig. 3. The SEM image of ACF (Fig. 3a) displays a regular smooth surface; meanwhile, that of L-cyst-ACF (Fig. 3b) shows an irregular rough surface after modification, which illustrates that organofunctional groups were successfully grafted. Alternatively, a larger specific surface area is also conducive to an improvement in adsorption capability. The changes on the surface of the modified ACF after adsorption are showed in Fig. 3(c and d). It can be observed that some irregular tiny particles covered the surface of the fibers after adsorption, demonstrating the further improved effective adsorption ability of L-cyst-ACF to remove Pb^{2+} ions.

The energy dispersive X-ray spectroscopy mapping of L-cyst-ACF is displayed in Fig. 4, which authenticated the presence of elements including carbon (C), oxygen (O), sulfur (S) and nitrogen (N) related to the presence of L-cysteine modified on ACF. As shown as Fig. 4(B–F), the successful grafting reaction of functional groups occurred on ACF. According to the data, it can be concluded that O and N are not co-localized with Pb. Fig. 4E and F show strong S and Pb signals, respectively, which are co-localized, suggesting that the primary adsorbent for Pb is S and that N and O did not significantly contribute to the adsorption.

Fig. 5A reveals the chemical composition changes in the modified activated carbon fibers compared with the original fiber according to the XPS analysis. The presence of amine groups confirmed that the grafting reaction occurred.
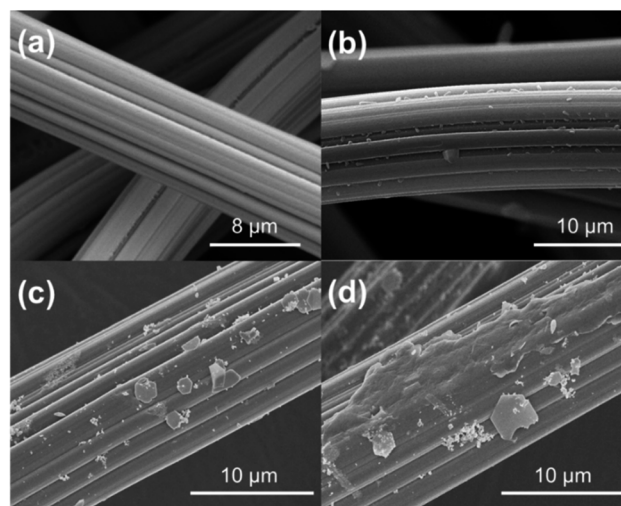

Fig. 2   FT-IR spectra of activated carbon fibers and L-cysteine-modified activated carbon fibers.

Fig. 3   SEM images of ACF and L-cyst-ACF (a) original ACF, (b) L-cyst-ACF (c and d) after Pb^{2+} adsorbed on L-cyst-ACF.
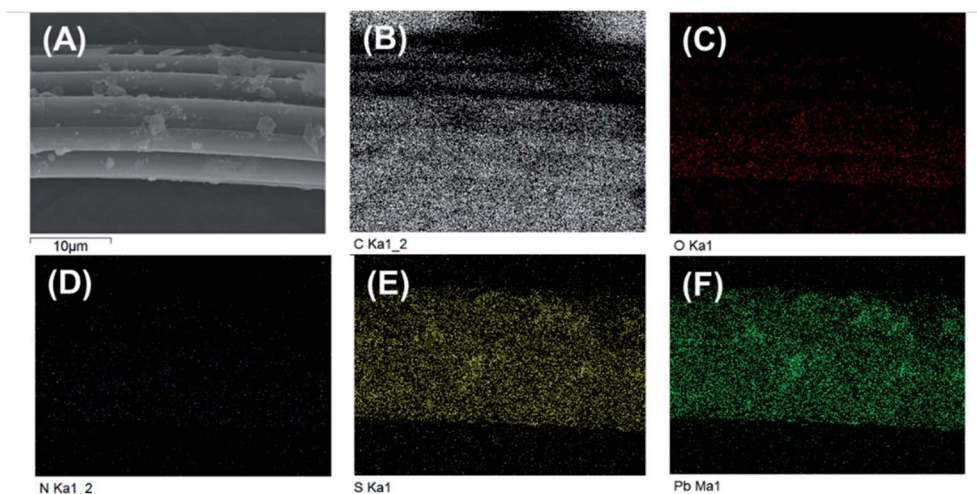
Fig. 4 (A) SEM image of ʟ-cyst-m-ACF after adsorption (B)–(F) EDS mapping of ʟ-cyst-m-ACF of C, O, S, N, and Pb elements after the adsorption of Pb^{2+}.
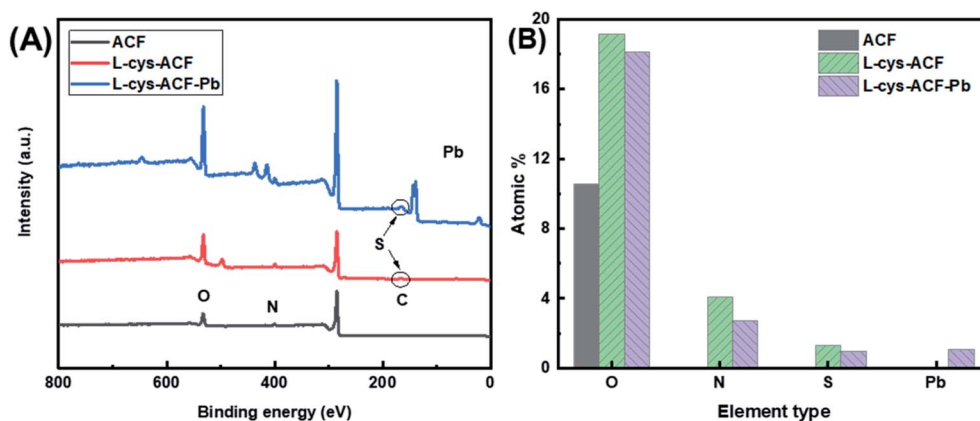

Fig. 5 (a) XPS spectra of base ACF, ʟ-cyst-ACF and ʟ-cyst-ACF-Pb. (b) Composition of fiber samples determined by XPS analysis.

Additionally, the ratio of different elements illustrates that the organic functional groups were successfully grafted, as shown in Fig. 5B. EDS mapping, FT-IR, and XPS analyses were employed to confirm the adsorption of Pb^{2+} on ʟ-cyst-ACF.

3.3 Lead adsorption

3.3.1 Contact time. The exploration of the adsorption equilibrium time is a crucial part of measuring the performance of an adsorbent and it is significance for subsequent research.[29] The change in the adsorption of the material with contact time is presented in Fig. 6. It shows that the adsorption capacity of Pb^{2+} increased rapidly within the first hour, which can be ascribed to the effective complexation of organic groups with Pb^{2+}.[30,31] Then, it remained at approximately 125 mg g^{-1} for Pb^{2+} after 6 h, indicating that adsorption equilibrium had been achieved.

3.3.2 Different adsorbent dosages. The removal efficiency of Pb^{2+} with different adsorbent dosages was also investigated. As shown in Fig. 7, the removal rate of Pb^{2+} increased significantly as the dosage increased. When the dosage increased from 0.25 g L^{-1} to 0.5 g L^{-1}, the removal of Pb^{2+} increased from 23.78% to 51.55%. Simultaneously, the degradation rate of Pb^{2+} did not increase significantly with an increase in the adsorption dosage. However, the removal efficiency of ʟ-cyst-ACF was limited when the adsorption dosage was greater than 0.5 g L^{-1}, indicating that a larger adsorption dosage had a greater impact on the further removal of Pb^{2+}. Thus, we chose the dosage of ʟ-cyst-ACF to be 0.5 g L^{-1} for the subsequent removal process.

3.3.3 Initial pH. Research has shown that the surface charge of the absorbent material, the degree of ion migration and the state of the adsorbed substance are affected by the pH of the solution during the adsorption process.[32] Fig. 8a shows that the amount of adsorption observably increased with an increase in pH. This phenomenon demonstrated that the existence of a large amount of H$^+$ ions competed with Pb^{2+} ions for the adsorption sites in the material in an acidic environment.[31] It is generally believed that lead ions exist as cations in aqueous solutions.[33,34] However, Pb^{2+} ions easily form $Pb(OH)_2$
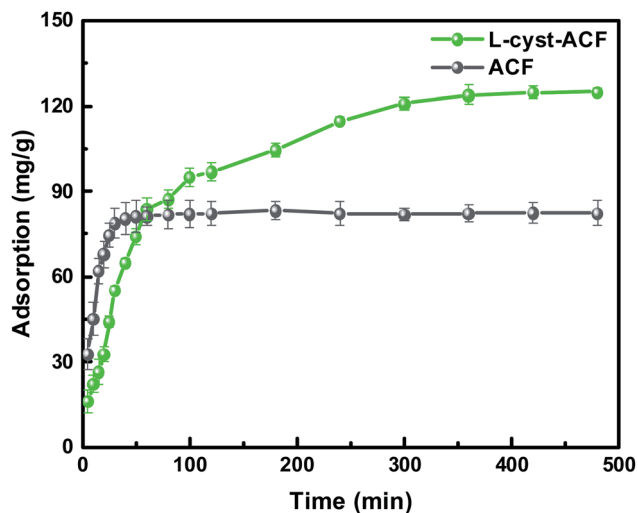
Fig. 6 Effect of contact time on the adsorption capacity of Pb^{2+} (pH = 5.5, temperature = 303 K, C_0 = 100 mg L^{-1}, and V = 100 mL).
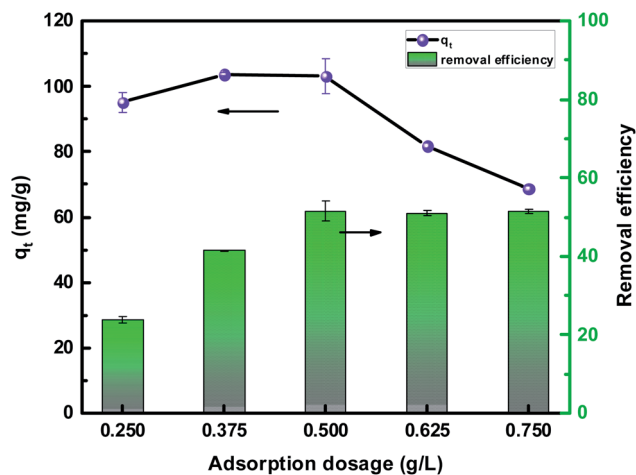

Fig. 7 Effect of different adsorbent dosages on the adsorption capacity and removal efficiency of Pb^{2+} (C_0 = 100 mg L^{-1}, V = 100 mL, contact time = 6 h, and temperature = 303 K).

(precipitation) with OH^- when the pH is greater than 6.[35] Thus, zeta potential (ζ) measurements at different pH were performed to explore the surface charge of the absorbent, as shown in Fig. 8b. Fig. 8b shows that the surface of the material exhibited a negative charge state as the pH increased. Because the functional groups such as $-NH_2$ and $-SH$ on the material surface lost H^- ions as the OH^- gradually increased in the solution, and they became the active state.[36] This active state was conducive to the adsorption of Pb^{2+} ions by the material. On the contrary, the hydroxyl, carboxyl, amine and sulfhydryl groups on the surface of L-cyst-ACF tended to be protonated, and they were positively charged when the pH value was low, which led to electrostatic repulsion between the binding site and Pb^{2+} ions.[15,37,38] Therefore, the pH of the solution and the surface charge of the material were the key factors that affected its adsorption capacity.

3.4 Adsorption kinetics

To quickly and accurately interpret the adsorption behavior of materials, four types of kinetic models were adopted in this investigation. The linear types of models are expressed as eqn (3)–(6).[39,40]

$$\ln(q_e - q_t) = \ln q_e - K_1 \cdot t \tag{3}$$

$$\frac{t}{q_t} = \frac{1}{K_2 \cdot q_e^2} + \frac{t}{q_e} \tag{4}$$

$$q_t = K_i \cdot t^{\frac{1}{2}} + a \tag{5}$$

$$q_t = \frac{1}{\beta}\ln(\alpha \cdot \beta) + \frac{1}{\beta}\ln t \tag{6}$$

where q_e and q_t are the adsorption capacity at equilibrium and time t (mg g^{-1}).[36] K_1 (min^{-1}) and K_2 [g·(mg min)$^{-1}$] are the rate constant. K_i is the rate constant of diffusion particles.[41] α [mg (g min)$^{-1}$] and β (g mg^{-1}) represent the initial constant adsorption and desorption constants, respectively.[42]

According to the fitting results in Fig. 9 and Table 1, it can be seen that the R^2 values of the pseudo-second-order and intra-particle-diffusion kinetic models were better than that of the
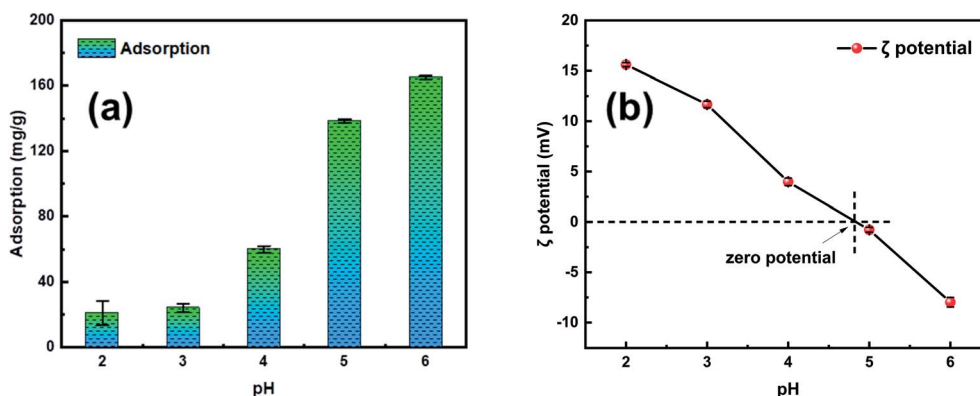

Fig. 8 Effect of initial pH on Pb^{2+} adsorption and zeta potential of L–cyst-ACF during removal process at different pH.
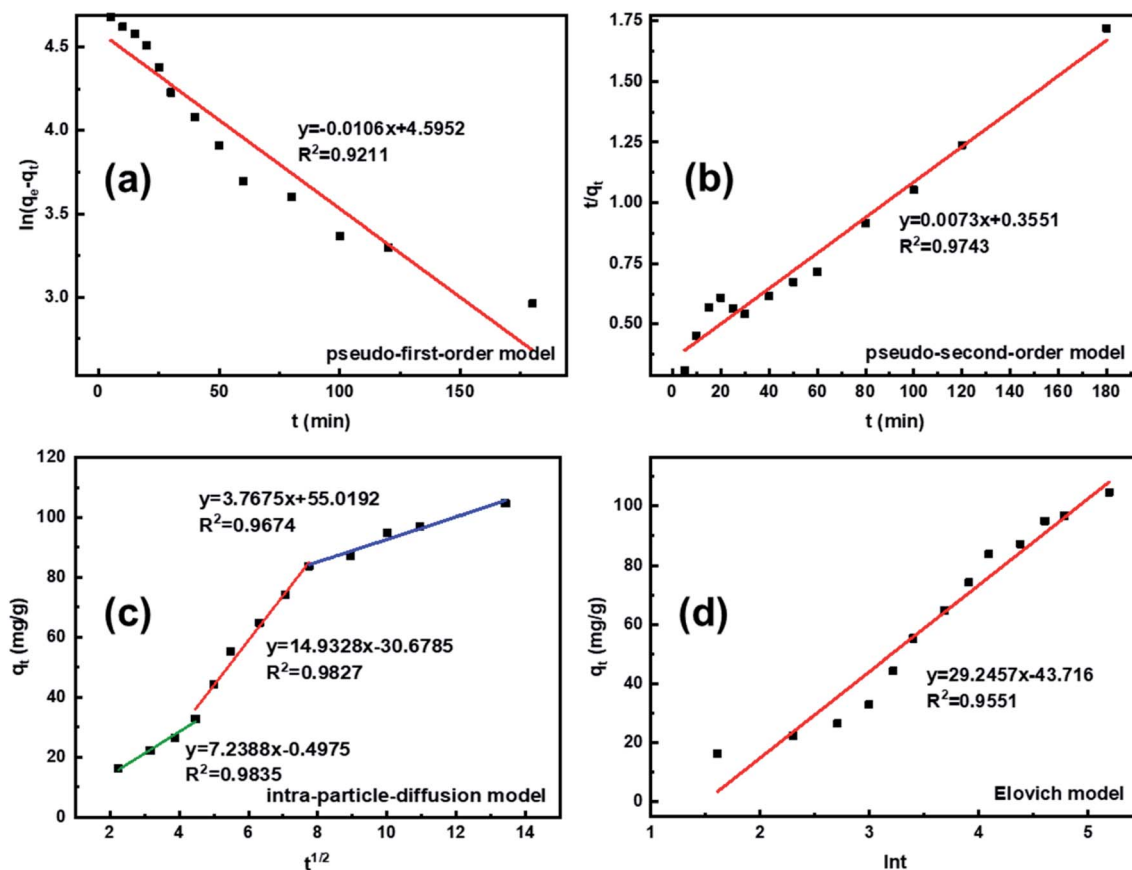
Fig. 9 (a) Plots of pseudo-first-order kinetic model for the adsorption of Pb^{2+}, (b) pseudo-second-order kinetic model for the adsorption of Pb^{2+}, (c) intra-particle-diffusion kinetic model for the adsorption of Pb^{2+}, (d) Elovich kinetic model for the adsorption of Pb^{2+}. Conditions: $T = 303$ K [adsorbent] = 0.5 g L^{-1} [metal] = 100 mg L^{-1}, pH = 5.5, and contact time = 6 h.

Table 1 The parameters of four types of kinetic models

Kinetic model	Parameter	Value
Pseudo-first-order model	q_e (mg g^{-1})	99.01
	K_1 (min^{-1})	0.0106
	R^2	0.9211
Pseudo-second-order model	q_e (mg g^{-1})	136.80
	K_2 [g·(mg min)$^{-1}$]	0.0073
	R^2	0.9743
Intraparticle diffusion model	K_1 [mg·(g·min$^{1/2}$)$^{-1}$]	7.2388
	K_2 [mg·(g·min$^{1/2}$)$^{-1}$]	14.9328
	K_3 [mg·(g·min$^{1/2}$)$^{-1}$]	3.7675
Elovich model	α [mg·(g min)$^{-1}$]	6.5584
	β (g mg^{-1})	0.0342
	R^2	0.9551

pseudo-first-order kinetic models and Elovich model, indicating that the possible mechanism of adsorption is chemisorption and the adsorbent surface corresponds to a heterogeneous system. Furthermore, this result reveals that the adsorption is related to the electron exchange between the surface functional groups and Pb^{2+} ions. The experimental equilibrium adsorption capacity, q_e (136.80 mg g^{-1}), obtained by fitting the pseudo-second-order kinetic equation maintained high consistency with the actual test value (~125 mg g^{-1}).

To investigate the internal diffusion mechanism during the adsorption process, the intra-particle diffusion model proposed by Weber and Morris[43] was used to discuss the rate-controlling step. Multi-linearity was observed, as shown in Fig. 9c, and the crucial information obtained is presented in Table 1. As shown in Fig. 9c, the Pb^{2+} adsorption process involved three steps. The initial linear part was the result of adsorption on the external surface, namely, the attachment of Pb^{2+} to the surface of L-cyst-ACF.[44] The second linear part represents the progressive internal diffusion of particles.[12] In the third part, the decreased diffusion rate is due to the reduction in Pb^{2+} concentration and the enhanced electrostatic repulsion on the material surface.[45] The intra-particle diffusion and complex or ion exchange may play a certain role in the adsorption process given that none of the three linear curves passed through the origin of the coordinate.[23] Combined with the characterization test and mechanism investigation, we realized that the relatively rough surface on the fiber surface and the partially oxidized thiol functional groups generated sulfonic acid groups, which reduced contact probability between the Pb^{2+} in solution and active sites on the material surface, affecting the transfer rate of Pb^{2+} in the surface liquid layer. Comparatively, the ion transport rate in the pore was larger. The α and β constants also indicated that the

material had a low adsorption rate and a non-homogeneous surface structure.

3.5 Adsorption isotherms

Two common isothermal models were used to evaluate the adsorption behavior between Pb^{2+} and L-cyst-ACF. The linear form of the Langmuir isotherm is represented by the following equation:[46]

$$\frac{C_e}{q_e} = \frac{1}{q_{max}} C_e + \frac{1}{K_L \cdot q_{max}} \tag{7}$$

where q_e and q_{max} represent the equilibrium adsorption capacity and monolayer maximum adsorption capacity (mg g^{-1}), respectively.[18] The constant K_L describes the affinity between the adsorbent and the target substance.[12]

The Freundlich model is described by the following equation:[46,47]

$$\log q_e = \log K_F + \frac{1}{n} \log C_e \tag{8}$$

where K_F and $1/n$ are empirical constants expressed the adsorption intensity and $\dfrac{\text{adsorb rate}}{\text{desorb rate}}$.[48]

The experimental results obtained by fitting the Langmuir and Freundlich models are shown in Fig. 10. The affinity and adsorption capacity of L-cyst-ACF for Pb^{2+} at different temperatures were evaluated. The constants for the two models are summarized in Table 2. The Langmuir model is normally used to evaluate the monolayer adsorption characteristics and energy level of a homogeneous material surface.[49] The R^2 value from the Langmuir model was higher than that from the Freundlich model, which indicates the adsorption of Pb^{2+} was primarily homogeneous and monolayer adsorption. The low K_L value suggests a relatively strong interaction between Pb^{2+} and L-cyst-ACF. Compared with the results in other works, as shown in Table 3, that herein exhibited a higher adsorption effect. The Freundlich model generally describes the multi-layer adsorption of the adsorbent on a heterogeneous surface and that the energy level of the adsorption site is not constant.[43] Meanwhile, the poor fitting data showed that the adsorption was not

Table 2 The parameters of the isotherm models

Isotherm models	Parameters	303 K	313 K	323 K
Langmuir model	q_{max} (mg g^{-1})	161.03	167.78	179.53
	K_L (L mg^{-1})	0.1021	0.1342	0.0481
	R^2	0.992	0.991	0.991
Freundlich model	K_F (L mg^{-1})	51.9481	57.4619	38.4964
	$1/n$	0.2201	0.196	0.2644
	R^2	0.967	0.883	0.857

physical adsorption or multilayer adsorption. Furthermore, the value of $1/n$ in the three ranges of $0 < 1/n < 1$, $1/n = 0$ and $1/n > 1$ implies favorable, unfavorable and irreversible adsorption, respectively.[50] Thus, it can be predicted that the adsorption behavior was favorable and spontaneous according to the fitting results.

3.6 Adsorption thermodynamics

The standard Gibbs free energy change (ΔG^θ), entropy change (ΔS^θ) and enthalpy change (ΔH^θ) were calculated using eqn (9) and (10) to recognize the energetics and spontaneity involved in the procedure for the combination of Pb^{2+} and the adsorbent.

$$\ln K^\theta = -\frac{\Delta H^\theta}{RT} + \frac{\Delta S^\theta}{R} \tag{9}$$

$$\Delta G^\theta = -R \cdot T \cdot \ln K^\theta \tag{10}$$

where K^θ represents the constant associated with the thermodynamic equilibrium, which is replaced by K_L from the Langmuir fitting.[43] R and T are the universal gas constant [8.314 J (mol^{-1} K^{-1})] and the temperature, respectively.[13]

The thermodynamic parameters of adsorption provide an effective method for in-depth understanding of the nature of the adsorption process. The changes on Gibbs free energy (ΔG), enthalpy (ΔH), and entropy (ΔS) values during Pb^{2+} adsorption was given in Table 4. Accordingly, the calculated adsorption enthalpy and entropy for of Pb^{2+} adsorption were positive, which indicated that the affinity between metal ions and the
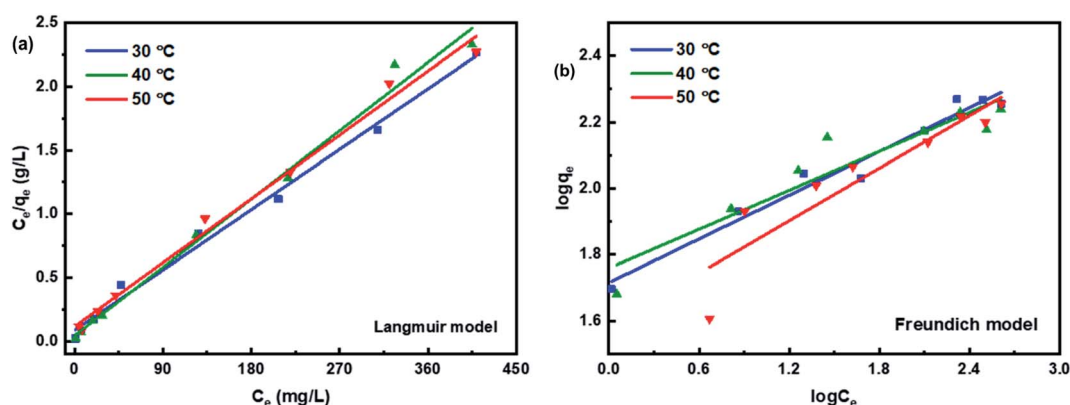

Fig. 10 Adsorption isotherms from (a) Langmuir and (b) Freundlich isotherm models for the adsorption of Pb^{2+} on the L-cyst-ACF composite. Conditions: [adsorbent] = 0.5 g L^{-1} [metal] = 100 mg L^{-1}, contact time = 6 h, and pH = 5.5.

Table 3 The comparison of the effect of different adsorption materials

Adsorbent	Fitting model	q_{max} mg g^{-1}	Ref.
Sulfur-ferromagnetic nanoparticles	Langmuir	66.45	51
Chitosan-gelatin aerogels	Langmuir	11.1	52
Agro waste biochar	Freundlich	119.8	53
Microwave-assisted rice straw activated carbon	Langmuir	152.39	54
Nonwoven polyethylene-coated polypropylene fiber	Langmuir	63.36	55
Activated carbon nanofiber	Freundlich	120.3	56
Nitrogen-doped carbon nanofibers	Langmuir	88	57
L-Cysteine-modified activated carbon fiber	Langmuir	179.53	This study

Table 4 Thermodynamic parameters for the adsorption of Pb^{2+}

Parameter	298 K	308 K	318 K
ΔG^{θ} (kJ mol^{-1})	−5.75	−5.23	−8.15
ΔH^{θ} (kJ·mol^{-1})		18.83	
ΔS^{θ} (J mol^{-1} K^{-1})		43.56	

material surface was sufficient to make it adhere, and the randomness of the solid-liquid interface increased during this process. Otherwise, negative ΔG value showed the feasibility and spontaneity of the adsorption process, indicating endothermic process which was also predicted before. The endothermic nature of adsorption could be attributed to the increasing temperature that accelerated the diffusion of Pb^{2+} and the increase of system disorder, which lead to the positive progress of adsorption.

3.7 Adsorption mechanism

The adsorption of metal ions on the surface of carbon materials is primarily related to their pore structure and surface groups. According to Fig. 11, the XPS spectra of L-cyst-ACF before and after adsorbing were recorded to gain insight into the mechanism of action between Pb^{2+} and L-cyst-ACF. The peak positions of Pb 4f 7/2 and Pb 4f 5/2 were detected at 143.78 and 139.03 eV, respectively, which indicate the successful adsorption of Pb^{2+}.[58] As shown in Fig. 11c, the binding energies of C 1s appeared at 284.74, 286.02 and 287.16 eV, which are ascribed to the C–C, C–O, and C=O bonds, respectively.[59] Subsequently, the peaks located at 284.63 and 285.35 eV are assigned to C–C and C–O, respectively, suggesting that both bonds almost did not play a role in the adsorption process. Notably, the peak position at 287.16 eV shifted to a higher position at 288.33 eV, which illustrates that the adsorption depends on the C=O bond.

The high-resolution XPS spectra of O 1s and N 1s before and after the adsorption of Pb^{2+} are showed in Fig. 11e–h. According to Fig. 11e, three peaks appeared at 531.17, 532.82, and 535.29 eV, which are attributed to the C–O, O=C–NH–, and O=C–O bonds, respectively.[60] Then, it was clearly demonstrated that the bonding energy positions at 531.94 and 532.93 eV did not change, which suggests that the covalent bonds of C–O and O=C–NH– are not involved in the adsorption process. The peak at 535.29 eV shifted to 534.07 eV, which

illustrates that the carboxyl group (O=C–O–) played a key role during the adsorption process. According to reports, a variety of carbonyl-containing oxygen functional groups, carboxylate and epoxide groups in the adsorbent structure act as electron donors, which lead to surface complexation with metal ions, contributing to the uptake of Pb^{2+}.[15,37,61]

There are three main binding energy positions at 398.63, 399.94, and 401.28 eV in Fig. 11g, which correspond to –NH, C–N, and O=C–NH–, respectively.[62] Obviously, these binding energy positions did not exhibit a visible change, as shown in Fig. 11h, which indicates that nitrogen-containing functional groups did not participate in the adsorption process. There are many chemical environments of S in the modified fiber material,[26] such as S–S, C–S, –SH, C=S, and SO$_3^{2-}$, which were accurately found at 163.74, 164.61, 167.53, 169.05, and 169.95 eV in Fig. 11i, respectively.[26,27] As shown in Fig. 11j, the spectra of S–S and C–S could be fitted with two peaks at 163.45 and 164.31 eV, which represent that these two bonds did not participate in the adsorption of Pb^{2+}. Surprisingly, the binding energy positions at 167.53, 169.05, and 169.95 shifted to lower positions, as shown in Fig. 11j (~165.57 eV, ~167.85 eV, and ~169.08 eV), revealing that –SH, C=S, and SO$_3^{2-}$, respectively, produced coordinated chelation and electrostatic attraction toward Pb^{2+}. According to the hard soft acid base (HSAB) theory,[63] a metal–ligand complex can be formed between Pb^{2+} (soft acid with empty track) and surface functional groups, such as –SH, O=C–O–, and C=S (soft base with free electrons) via covalent bonding. Therefore, the formation of metal–organic complexes greatly improved the adsorption properties of the material.

3.8 Reusability and cycling performance

It was very important to evaluate the cycling performance of L-cyst-ACF considering the cost of adsorbents used in practical production. Therefore, adsorption–desorption cycle experiments were carried out on L-cyst-ACF herein, focusing on the reusability and removal efficiency changes. EDTA-2Na salt solution with a concentration of 0.5 mol L^{-1} was used to desorb L-cyst-ACF saturated with adsorbed species in this study. The changes in the adsorption capacity and adsorption efficiency of the material after 5 adsorption–desorption cycles are summarized in Fig. 12. With an increase in the number of regeneration cycles, the adsorption of lead ions decreased from
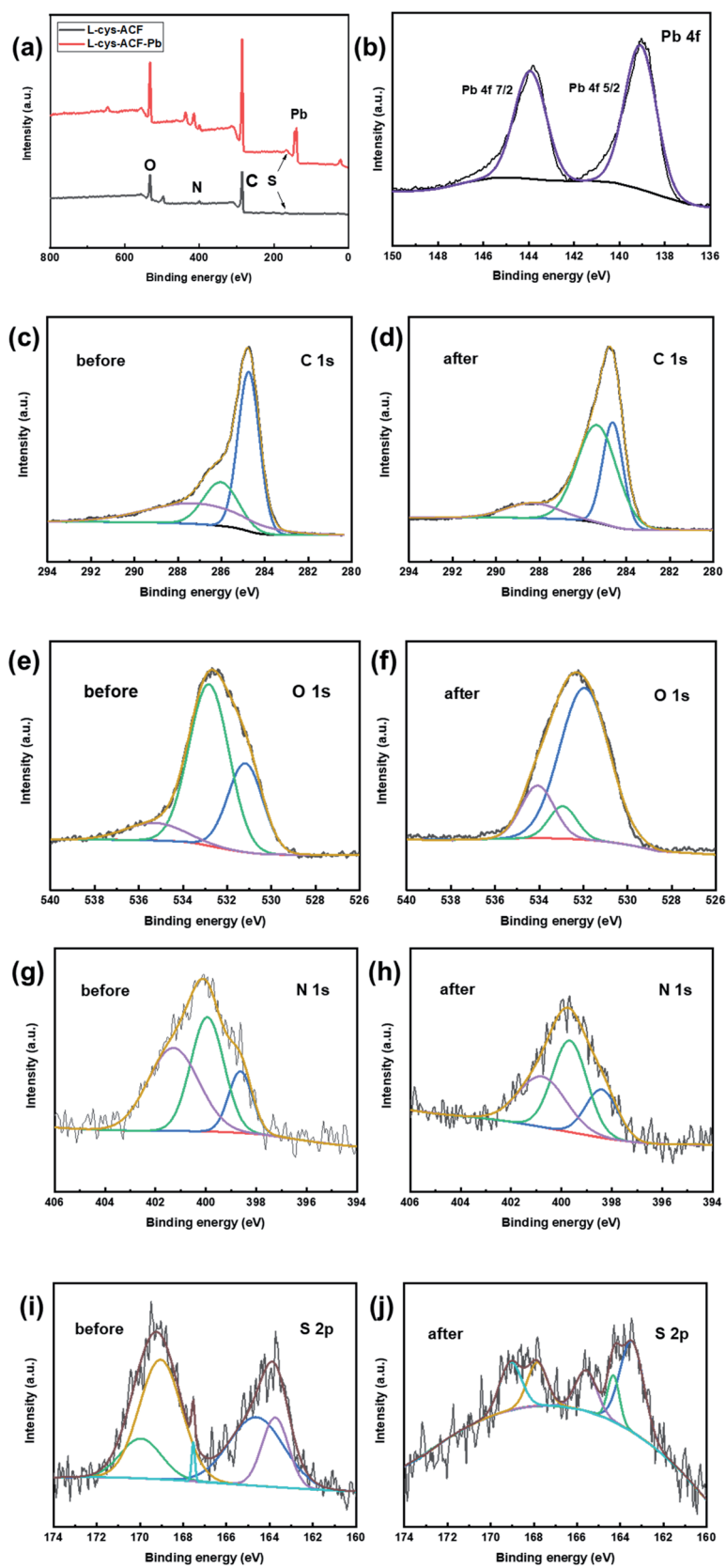
Fig. 11 XPS spectra of (a) full survey (b) Pb 4f and (c and d) C 1s (e and f) O 1s (g and h) N 1s and (i and j) S 2p before and after adsorption, respectively.
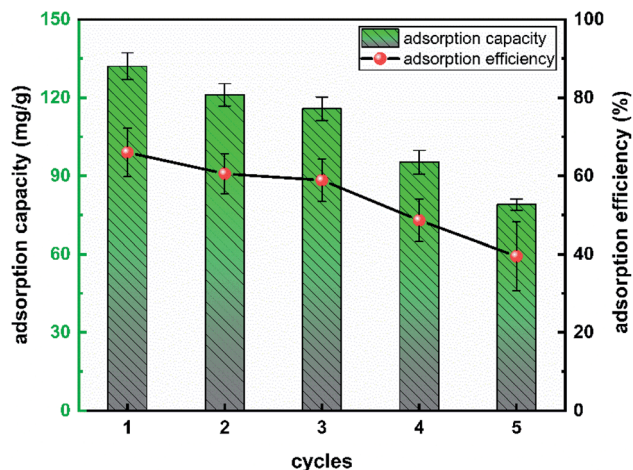
Fig. 12 Reusability performance of L-cyst-ACF-adsorbed Pb^{2+}.

about 130 mg g^{-1} to only 80 mg g^{-1}, indicating that the adsorption capacity of L-cyst-ACF for Pb^{2+} decreased after the fiber underwent multiple elution cycles. We speculated that the functional groups on the fiber surface were lost and some were oxidized and failed during repeated experimental operations. In general, L-cyst-ACF exhibited ideal reusability and has certain prospects in the treatment of lead pollution.

4 Conclusion

An activated carbon fiber material grafted with L-cysteine was prepared *via* an amide reaction and the batch adsorption experiments showed that L-cyst-ACF was effective for the removal of Pb^{2+} from aqueous solution. Adsorption experiments were carried out to investigate different factors such as initial concentration, pH, adsorbent dosage, contact time, and temperature. The experimental results showed that the adsorption effect was better when the pH of the solution was between 5 and 6; a higher temperature was conducive to the adsorption process; the adsorption efficiency was the best when the dosage of adsorbent was 0.5 g L; the adsorption reached equilibrium within 6 h, and q_e was 136.80 mg g^{-1}. In addition, L-cyst-ACF had a certain cycling performance after multiple regeneration treatments.

Compared with the pseudo-first-order kinetic equation, it was concluded that the fitting of the pseudo-second-order kinetic equation was more suitable in the adsorption process, implying that the adsorption process was chemisorption. The data from the isothermal models showed that the Langmuir model fitted well, which indicated that the material adsorption process was monolayer adsorption. The thermodynamic analysis showed that ΔG was negative at all temperatures, which indicated that the adsorption process was endothermic and spontaneous. The positive ΔS indicated that the system disorder gradually increased during the adsorption process. Finally, the XPS analysis illustrated that abundant –SH, –COOH, and C=S groups on the fiber surface were the crucial factor for the significant improvement in the adsorption capacity.

Conflicts of interest

The authors declare no competing financial interest.

References

1 R. M. Ali, H. A. Hamad, M. M. Hussein and G. F. Malash, Potential of using green adsorbent of heavy metal removal from aqueous solutions: Adsorption kinetics, isotherm, thermodynamic, mechanism and economic analysis, *Ecol. Eng.*, 2016, **91**, 317–332.

2 C. Men, R. Liu, F. Xu, Q. Wang, L. Guo and Z. Shen, Pollution characteristics, risk assessment, and source apportionment of heavy metals in road dust in Beijing, China, *Sci. Total Environ.*, 2018, **612**, 138–147.

3 X. Bi, Z. Li, G. Sun, J. Liu and Z. Han, In vitro bioaccessibility of lead in surface dust and implications for human exposure: A comparative study between industrial area and urban district, *J. Hazard. Mater.*, 2015, **297**, 191–197.

4 V. Matovic, A. Buha, D. Ethukic-Cosic and Z. Bulat, Insight into the oxidative stress induced by lead and/or cadmium in blood, liver and kidneys, *Food Chem. Toxicol.*, 2015, **78**, 130–140.

5 M. Thakur, S. Praveen, P. R. Divte, R. Mitra, M. Kumar, C. K. Gupta, *et al.* Metal tolerance in plants: Molecular and physicochemical interface determines the "not so heavy effect" of heavy metals, *Chemosphere*, 2022, **287**(Pt 1), 131957.

6 M. Hanna-Attisha, J. LaChance, R. C. Sadler and A. Champney Schnepp, Elevated Blood Lead Levels in Children Associated With the Flint Drinking Water Crisis: A Spatial Analysis of Risk and Public Health Response, *Am. J. Public Health*, 2016, **106**(2), 283–290.

7 R. Alizadeh, R. K. Kazemi and M. R. Rezaei, Ultrafast removal of heavy metals by tin oxide nanowires as new adsorbents in solid-phase extraction technique, *Int. J. Environ. Sci. Technol.*, 2017, **15**(8), 1641–1648.

8 M. Nemati, S. M. Hosseini, F. Parvizian, N. Rafiei and B. Van der Bruggen, Desalination and heavy metal ion removal from water by new ion exchange membrane modified by synthesized NiFe2O4/HAMPS nanocomposite, *Ionics*, 2019, **25**(8), 3847–3857.

9 M. C. Benalia, L. Youcef, M. G. Bouaziz, S. Achour and H. Menasra, Removal of Heavy Metals from Industrial Wastewater by Chemical Precipitation: Mechanisms and Sludge Characterization, *Arabian J. Sci. Eng.*, 2022, **47**(5), 5587–5599.

10 H. Alijani, M. H. Beyki, Z. Shariatinia, M. Bayat and F. Shemirani, A new approach for one step synthesis of magnetic carbon nanotubes/diatomite earth composite by

chemical vapor deposition method: Application for removal of lead ions, *Chem. Eng. J.*, 2014, **253**, 456–463.

11 Z.-f. Cao, X. Wen, J. Wang, F. Yang, H. Zhong, S. Wang, *et al. In situ* nano-Fe$_3$O$_4$/triisopropanolamine functionalized graphene oxide composites to enhance Pb^{2+} ions removal, *Colloids Surf., A*, 2019, **561**, 209–217.

12 J. Qu, Y. Liu, L. Cheng, Z. Jiang, G. Zhang, F. Deng, *et al.* Green synthesis of hydrophilic activated carbon supported sulfide nZVI for enhanced Pb(II) scavenging from water: Characterization, kinetics, isotherms and mechanisms, *J. Hazard. Mater.*, 2021, **403**, 123607.

13 E. Santoso, R. Ediati, Y. Kusumawati, H. Bahruji, D. O. Sulistiono and D. Prasetyoko, Review on recent advances of carbon based adsorbent for methylene blue removal from waste water, *Mater. Today Chem.*, 2020, **16**, 100233.

14 Y. Yang, Y. Xie, L. Pang, M. Li, X. Song, J. Wen, *et al.* Preparation of reduced graphene oxide/poly(acrylamide) nanocomposite and its adsorption of Pb(II) and methylene blue, *Langmuir*, 2013, **29**(34), 10727–10736.

15 L. X. Zhang, S. Y. Tang, F. X. He, Y. Liu, W. Mao and Y. T. Guan, Highly efficient and selective capture of heavy metals by poly(acrylic acid) grafted chitosan and biochar composite for wastewater treatment, *Chem. Eng. J.*, 2019, **378**, 122215.

16 A. A. Alqadami, M. Naushad, A. L. ZA, M. Alsuhybani and M. Algamdi, Excellent adsorptive performance of a new nanocomposite for removal of toxic Pb(II) from aqueous environment: Adsorption mechanism and modeling analysis, *J. Hazard. Mater.*, 2020, **389**, 121896.

17 P. S. Carraro, L. Spessato, L. H. S. Crespo, J. T. C. Yokoyama, J. M. Fonseca, K. C. Bedin, *et al.* Activated carbon fibers prepared from cellulose and polyester–derived residues and their application on removal of Pb^{2+} ions from aqueous solution, *J. Mol. Liq.*, 2019, **289**, 111150.

18 S. Deng, P. Wang, G. Zhang and Y. Dou, Polyacrylonitrile-based fiber modified with thiosemicarbazide by microwave irradiation and its adsorption behavior for Cd(II) and Pb(II), *J. Hazard. Mater.*, 2016, **307**, 64–72.

19 S. He, C. Lu and S. Zhang, Facile and efficient route to polyimide-TiO2 nanocomposite coating onto carbon fiber, *ACS Appl. Mater. Interfaces*, 2011, **3**(12), 4744–4750.

20 J. A. Arcibar-Orozco, J. R. Rangel-Mendez and P. E. Diaz-Flores, Simultaneous Adsorption of Pb(Ii)-Cd(Ii), Pb(Ii)-Phenol, and Cd(Ii)-Phenol by Activated Carbon Cloth in Aqueous Solution, *Water, Air, Soil Pollut.*, 2014, **226**(1), 2197.

21 N. Wang, Y. Qiu, T. Xiao, J. Wang, Y. Chen, X. Xu, *et al.* Comparative studies on Pb(II) biosorption with three spongy microbe-based biosorbents: High performance, selectivity and application, *J. Hazard. Mater.*, 2019, **373**, 39–49.

22 G. Xu, Y. J. Xie, J. Cao, M. L. Tao and W. Q. Zhang, Highly selective and efficient chelating fiber functionalized by bis(2-pyridylmethyl)amino group for heavy metal ions, *Polym. Chem.*, 2016, **7**(23), 3874–3883.

23 L. Sharma and R. Kakkar, Hierarchical Porous Magnesium Oxide (Hr-MgO) Microspheres for Adsorption of an Organophosphate Pesticide: Kinetics, Isotherm, Thermodynamics, and DFT Studies, *ACS Appl. Mater. Interfaces*, 2017, **9**(44), 38629–38642.

24 G. B. Adebayo, H. I. Adegoke and S. Fauzeeyat, Adsorption of Cr(VI) ions onto goethite, activated carbon and their composite: kinetic and thermodynamic studies, *Appl. Water Sci.*, 2020, **10**(9), 213.

25 Q. Jiang, W. Xie, S. Han, Y. Wang and Y. Zhang, Enhanced adsorption of Pb(II) onto modified hydrochar by polyethyleneimine or H3PO4: An analysis of surface property and interface mechanism, *Colloids Surf., A*, 2019, 583.

26 S. Pan, Y. Zhang, H. Shen and M. Hu, An intensive study on the magnetic effect of mercapto-functionalized nano-magnetic Fe3O4 polymers and their adsorption mechanism for the removal of Hg(II) from aqueous solution, *Chem. Eng. J.*, 2012, **210**, 564–574.

27 P. L. Yap, Y. L. Auyoong, K. Hassan, F. Farivar, D. N. H. Tran, J. Ma, *et al.* Multithiol functionalized graphene bio-sponge *via* photoinitiated thiol-ene click chemistry for efficient heavy metal ions adsorption, *Chem. Eng. J.*, 2020, **395**, 124965.

28 Y. Huang, Y. Gong, J. Tang and S. Xia, Effective removal of inorganic mercury and methylmercury from aqueous solution using novel thiol-functionalized graphene oxide/Fe-Mn composite, *J. Hazard. Mater.*, 2019, **366**, 130–139.

29 K. M. Mena Aguilar, Y. Amano and M. Machida, Ammonium persulfate oxidized activated carbon fiber as a high capacity adsorbent for aqueous Pb(II), *J. Environ. Chem. Eng.*, 2016, **4**(4), 4644–4652.

30 J. Mao, M. Ge, J. Huang, Y. Lai, C. Lin, K. Zhang, *et al.* Constructing multifunctional MOF@rGO hydro-/aerogels by the self-assembly process for customized water remediation, *J. Mater. Chem. A*, 2017, **5**(23), 11873–11881.

31 X. Yang, Y. Wan, Y. Zheng, F. He, Z. Yu, J. Huang, *et al.* Surface functional groups of carbon-based adsorbents and their roles in the removal of heavy metals from aqueous solutions: A critical review, *Chem. Eng. J.*, 2019, **366**, 608–621.

32 L. M. Cui, Y. G. Wang, L. Gao, L. H. Hu, L. G. Yan, Q. Wei, *et al.* EDTA functionalized magnetic graphene oxide for removal of Pb(II), Hg(II) and Cu(II) in water treatment: Adsorption mechanism and separation property, *Chem. Eng. J.*, 2015, **281**, 1–10.

33 C. J. Madadrang, H. Y. Kim, G. Gao, N. Wang, J. Zhu, H. Feng, *et al.* Adsorption behavior of EDTA-graphene oxide for Pb (II) removal, *ACS Appl. Mater. Interfaces*, 2012, **4**(3), 1186–1193.

34 K. G. Sreejalekshmi, K. A. Krishnan and T. S. Anirudhan, Adsorption of Pb(II) and Pb(II)-citric acid on sawdust activated carbon: Kinetic and equilibrium isotherm studies, *J. Hazard. Mater.*, 2009, **161**(2–3), 1506–1513.

35 N. N. Wang, X. J. Xu, H. Y. Li, J. L. Zhai, L. Z. Yuan, K. X. Zhang, *et al.* Preparation and Application of a Xanthate-Modified Thiourea Chitosan Sponge for the Removal of Pb(II) from Aqueous Solutions, *Ind. Eng. Chem. Res.*, 2016, **55**(17), 4960–4968.

36 P. L. Yap, K. Hassan, Y. L. Auyoong, N. Mansouri, F. Farivar, D. N. H. Tran, *et al.* All-in-One Bioinspired Multifunctional Graphene Biopolymer Foam for Simultaneous Removal of Multiple Water Pollutants, *Adv. Mater. Interfaces*, 2020, **7**(18), 2000664.

37 L. Zhou, L. Ji, P. C. Ma, Y. Shao, H. Zhang, W. Gao, *et al.* Development of carbon nanotubes/CoFe2O4 magnetic hybrid material for removal of tetrabromobisphenol A and Pb(II), *J. Hazard. Mater.*, 2014, **265**, 104–114.

38 L. Zhang, W. Li, H. Cao, D. Hu, X. Chen, Y. Guan, *et al.* Ultra-efficient sorption of Cu(2+) and Pb(2+) ions by light biochar derived from Medulla tetrapanacis, *Bioresour. Technol.*, 2019, **291**, 121818.

39 W. Rudzinski and W. Plazinski, Kinetics of dyes adsorption at the solid-solution interfaces: a theoretical description based on the two-step kinetic model, *Environ. Sci. Technol.*, 2008, **42**(7), 2470–2475.

40 J. Wang and X. Guo, Adsorption kinetic models: Physical meanings, applications, and solving methods, *J. Hazard. Mater.*, 2020, **390**, 122156.

41 J. Ai, F. Y. Chen, C. Y. Gao, H. R. Tian, Q. J. Pan and Z. M. Sun, Porous Anionic Uranyl-Organic Networks for Highly Efficient Cs(+) Adsorption and Investigation of the Mechanism, *Inorg. Chem.*, 2018, **57**(8), 4419–4426.

42 S. Kim, C. M. Park, M. Jang, A. Son, N. Her, M. Yu, *et al.* Aqueous removal of inorganic and organic contaminants by graphene-based nanoadsorbents: A review, *Chemosphere*, 2018, **212**, 1104–1124.

43 M. A. Al-Ghouti and D. A. Da'ana, Guidelines for the use and interpretation of adsorption isotherm models: A review, *J. Hazard. Mater.*, 2020, **393**, 122383.

44 Z. Liu, X. Zhong, Y. Wang, Z. Ding, C. Wang, G. Wang, *et al.* An Efficient Adsorption of Manganese Oxides/Activated Carbon Composite for Lead(II) Ions from Aqueous Solution, *Arabian J. Sci. Eng.*, 2017, **43**(5), 2155–2165.

45 G. Özsin, M. Kılıç, E. Apaydın-Varol and A. E. Pütün, Chemically activated carbon production from agricultural waste of chickpea and its application for heavy metal adsorption: equilibrium, kinetic, and thermodynamic studies, *Appl. Water Sci.*, 2019, **9**(3), 56.

46 J. Wang and X. Guo, Adsorption isotherm models: Classification, physical meaning, application and solving method, *Chemosphere*, 2020, **258**, 127279.

47 S. M. Khadivi, L. Edjlali, A. Akbarzadeh and K. Seyyedi, Enhanced adsorption behavior of amended EDTA-graphene oxide for methylene blue and heavy metal ions, *Int. J. Environ. Sci. Technol.*, 2019, **16**(12), 8151–8160.

48 M. Rethinasabapathy, S.-M. Kang, I. Lee, G.-W. Lee, S. K. Hwang, C. Roh, *et al.* Layer-Structured POSS-Modified Fe-Aminoclay/Carboxymethyl Cellulose Composite as a Superior Adsorbent for the Removal of Radioactive Cesium and Cationic Dyes, *Ind. Eng. Chem. Res.*, 2018, **57**(41), 13731–13741.

49 T. Bohli, A. Ouederni and I. Villaescusa, Simultaneous adsorption behavior of heavy metals onto microporous olive stones activated carbon: analysis of metal interactions, *Euro-Mediterr. j. environ. integr.*, 2017, **2**(1), 19.

50 S. Malamis and E. Katsou, A review on zinc and nickel adsorption on natural and modified zeolite, bentonite and vermiculite: examination of process parameters, kinetics and isotherms, *J. Hazard. Mater.*, 2013, **252–253**, 428–461.

51 H. Song, A. Kumar and Y. Zhang, A novel approach for the removal of Pb(2+) and Cd(2+) from wastewater by sulfur-ferromagnetic nanoparticles (SFMNs), *Chemosphere*, 2022, **287**(Pt 2), 132156.

52 A. Kovtun, E. Campodoni, L. Favaretto, M. Zambianchi, A. Salatino, S. Amalfitano, *et al.* Multifunctional graphene oxide/biopolymer composite aerogels for microcontaminants removal from drinking water, *Chemosphere*, 2020, **259**, 127501.

53 R. Gayathri, K. P. Gopinath and P. S. Kumar, Adsorptive separation of toxic metals from aquatic environment using agro waste biochar: Application in electroplating industrial wastewater, *Chemosphere*, 2021, **262**, 128031.

54 Z. Du, H. Chen, X. Guo, L. Qin, D. Lin, L. Huo, *et al.* Mechanism and industrial application feasibility analysis on microwave-assisted rapid synthesis of amino-carboxyl functionalized cellulose for enhanced heavy metal removal, *Chemosphere*, 2021, **268**, 128833.

55 F. Özmen, S. Korpayev, P. A. Kavaklı and C. Kavaklı, Activation of inert polyethylene/polypropylene nonwoven fiber (NWF) by plasma-initiated grafting and amine functionalization of the grafts for Cu(II), Co(II), Cr(III), Cd(II) and Pb(II) removal, *React. Funct. Polym.*, 2022, 174.

56 N. Abdullah, F. E. C. Othman, N. Yusof, T. Matsuura, W. J. Lau, J. Jaafar, *et al.* Preparation of nanocomposite activated carbon nanofiber/manganese oxide and its adsorptive performance toward leads (II) from aqueous solution, *J. Water Process. Eng.*, 2020, **37**, 101430.

57 A. Modi, B. Bhaduri and N. Verma, Facile One-Step Synthesis of Nitrogen-Doped Carbon Nanofibers for the Removal of Potentially Toxic Metals from Water, *Ind. Eng. Chem. Res.*, 2015, **54**(18), 5172–5178.

58 W. Czepa, D. Pakulski, S. Witomska, V. Patroniak, A. Ciesielski and P. Samori, Graphene oxide-mesoporous SiO2 hybrid composite for fast and efficient removal of organic cationic contaminants, *Carbon*, 2020, **158**, 193–201.

59 F. Cao and J. Shen, PEI-Modified CMKGM/GO Porous Biocomposite for Superior Removal of Pb(II), *J. Chem. Eng. Data*, 2019, **64**(12), 5622–5629.

60 H. Wang, X. Yuan, Y. Wu, X. Chen, L. Leng, H. Wang, *et al.* Facile synthesis of polypyrrole decorated reduced graphene oxide–Fe$_3$O$_4$ magnetic composites and its application for the Cr(VI) removal, *Chem. Eng. J.*, 2015, **262**, 597–606.

61 J. Kolarik, A. Bakandritsos, Z. Bad'ura, R. Lo, G. Zoppellaro, S. Kment, *et al.* Carboxylated Graphene for Radical-Assisted Ultra-Trace-Level Water Treatment and Noble Metal Recovery, *ACS Nano*, 2021, **15**(2), 3349–3358.

62 Y. H. Liao, Y. Q. Wang, X. F. Zhu and G. D. Ji, Amide-functionalized graphene-assembled monoliths with high adsorption capacity of Cd2+, *Environ. Technol. Innovation*, 2021, **23**, 00228-5.

63 T.-L. Ho, Hard soft acids bases (HSAB) principle and organic chemistry, *Chem. Rev.*, 2002, **75**(1), 1–20.